Applied Catalysis B: Environmental 195 (2016) 77–89

Contents lists available at ScienceDirect

Applied Catalysis B: Environmental

journal homepage: www.elsevier.com/locate/apcatb

Elucidating the field influence on the energetics of the methane steam reforming reaction: A density functional theory study

Fanglin Che [a], Su Ha [a], Jean-Sabin McEwen [a,b,c,*]

[a] The Gene and Linda Voiland School of Chemical Engineering and Bioengineering, Washington State University, WA 99164, United States
[b] Department of Physics and Astronomy, Washington State University, WA 99164, United States
[c] Department of Chemistry, Washington State University, WA 99164, United States

ARTICLE INFO

Article history:
Received 24 February 2016
Received in revised form 12 April 2016
Accepted 14 April 2016
Available online 29 April 2016

Keywords:
Methane steam reforming
Low operating temperatures
Electric fields
Electrocatalysis
Phase diagram

ABSTRACT

To help realize lower operating-temperatures for the highly endothermic Ni-catalytic methane steam reforming (MSR) process, we focused on elucidating the influence of an applied electric field on the energetics of the said reaction. Two aspects were considered in this study: the electric field effects on (i) the adsorption and electronic properties of the MSR-involved species, and (ii) the overall MSR energy profile. Our results show that for Ni-based MSR processes, a positive field strengthens the adsorption of the reactants, promotes product desorption, impedes coke formation, lowers the overall energy profiles and consequently, reduces the temperature requirements for the overall MSR-on-Ni reaction. Based on our phase diagram obtained from first principles, we show that CO can be obtained from the dehydrogenation of COH and CHO at moderate hydrogen partial pressure values with a negative field, while methanol is formed on the surface via hydroxyl oxidation of CH_3 at high hydrogen partial pressures and positive field values. This investigation suggests ways to facilitate the MSR reforming reaction in the presence of an electric field and also points toward a number of elementary reactions that need to be considered for establishing microkinetic model studies.

1. Introduction

Hydrogen, the energy carrier of the future, can be used in various applications (e.g. vehicles and fuel cells) [1] and cater to our dramatically growing need for sustainable energy resources as well as our ever-present environmental concerns. To generate hydrogen, steam reforming of natural gas (methane) over Ni-based catalysts is widely employed in industry [2,3]. In addition, methane steam reforming (MSR) is a reaction of interest since it can also be performed directly at the anode of a solid oxide fuel cell (SOFC) to generate electric power in the direct internal reforming reaction, which couples steam reforming with subsequent syngas electrochemical oxidation [4–6]. However, the main issue for the said reaction is that methane (CH_4) is very thermodynamically stable and requires a large amount of energy to break its C—H bonds, which makes the MSR reaction a highly endothermic process requiring temperatures of 900 K or higher [7]. Consequently, the Ni catalyst is placed in expensive alloy tubes to tolerate the extremely high thermal fluxes that will occur through the tube walls of the reactor [8,9]. An additional problem related to the high operating-temperature requirements involved in the MSR reaction is the increased occurrence of sintering [10,11] and coking [12–14], which reduces the lifetime of the Ni catalysts. To rationally design catalysts with lower temperature requirements for a methane reformer in industrial or fuel cell applications, it is necessary to understand the thermodynamic properties of the Ni-based MSR reaction at the atomic scale.

The kinetic and thermodynamic properties of methane steam reforming are well studied [15–19]. Jones et al. showed that the dissociative adsorption of CH_4 and the formation of CO are the rate-limiting steps over different transition metals supported by Al_2O_3 and ZrO_2 under MSR conditions from both first principles calculations and experimental investigations [20]. The CO formation barrier is found to be the dominant rate-limiting step at lower temperatures (773 K), while the dissociative adsorption barrier for CH_4 is dominant at higher temperatures above 873 K. Bengaard et al. [21] proposed a possible mechanism over pure Ni catalysts, which is shown in Eq. (1).

$$CH_4 + H_2O \rightarrow C + 4H + H_2O \rightarrow C + 6H + O \rightarrow CO + 3H_2 \quad (1)$$

* Corresponding author at: The Gene and Linda Voiland School of Chemical Engineering and Bioengineering, Washington State University, WA 99164, United States.
E-mail address: js.mcewen@wsu.edu (J.-S. McEwen).

http://dx.doi.org/10.1016/j.apcatb.2016.04.026
0926-3373/

Their data indicates that C and CH species are the most stable intermediates on Ni(111) and Ni(211). The overall calculated MSR reaction energy for forming syngas, the total energy differences between the reactant ($CH_4 + H_2O$) and the product ($CO + H_2$) in the gas phase, is 3.03 eV. After correcting the zero-point energies as well as the variation of the enthalpy of the said reaction at T = 298.15 K ($\Delta C_p \Delta T$) [22], the corresponding reaction enthalpy for the said reaction is 2.38 eV, which is in good agreement with the experimental value of 2.14 eV. Using DFT calculations, Blaylock's et al. [23] developed a microkinetic model to investigate the MSR reaction on a Ni(111) surface under realistic conditions. Similar to Rostrup-Nielsen's work [24], they found that CH is the most important carbon-containing reaction intermediate. Wang et al. [25]. studied the stabilities of the intermediates during the CO_2 reforming of CH_4 and found that O, CH_3, CH_2, CH and CHO were key intermediates, in which the most favorable mechanism is as follows:

$$CH_4 + CO_2 \rightarrow CH + 3H + CO + O \rightarrow CHO + 3H + CO \rightarrow 2CO + 4H \quad (2)$$

However, thus far, the influence of the environment on the underlying reaction mechanism over heterogeneous catalysts is still largely unexplored. One possible route to achieve lower operating-temperature requirements for the MSR reaction is to study the effects of the electric field on its mechanism [26–28]. Gorin et al. applied interfacial electric fields, generated from a parallel plate cell with a voltage source, to the Al_2O_3 catalytic rearrangement of *cis*-stilbene oxide. The results showed that the reaction conversion of the cis-stilbene oxide to the aldehyde and ketone products increased up to 10 times higher in the presence of an interfacial electric field as compared to when such as field is absent. Further, the aldehyde to ketone product ratio increased from 1:4 (without electric fields) to 17:1 (in the presence of an electric field) [26]. Sekine et al. investigated the electric field effects on the methane steam reforming over Pd/CeO_2, Ru/CeO_2 and Pt/CeO_2 catalysts, so called "electro-reforming" [27,28]. The methane conversion was largely enhanced with an electric field over all catalysts as well as the hydrogen production yields. Furthermore, our previous work concluded that a positive field could significantly reduce pure carbon deposits over Ni catalysts by decreasing the stabilities of pure carbon atoms and increasing the activation energy barrier for CH dissociation. In addition, the presence of a positive field strengthened the adsorption of H_2O, while a negative electric field had an opposite effect. Moreover, we examined methane and water dissociation over flat and stepped Ni surfaces and found similar electric field effects on both Ni surfaces for the above-mentioned reactions [29–31].

There are several approaches to apply an electric field in the theoretical work, such as the Neugebauer and Scheffler's method [32] (NS) and the double reference method of Neurock and coworkers [33,34]. For the NS approach [32], one inserts a dipole sheet in the middle of the vacuum of a supercell to polarize the metal surface. The polarization induces opposite charges on the top and bottom of the metal surfaces and thereby generates a uniform electric field (F) at a given specified value. With this approach, the interaction between the metal and the adsorbate depends on the effective dipole moment and the effective polarizability of the system. Large electric fields, on the order of ±1 V/Å, can rearrange the molecular or atomic orbitals of the intermediates, which can directly alter the stabilities of the reaction intermediates and consequently change the underlying reaction mechanism [35–37]. To relate the applied field to the electrode potential, a rough approximation based on a Helmholtz model proposed by Janik and coworkers was proposed [38,39]:

$$F = \frac{(U - U(PZC))}{d} \quad (3)$$

where d is the distance between the electrode surface and counter-ion charge plane (i.e. the thickness of the Helmholtz layer of a fuel cell system). U(PZC) is the potential of zero charge, which varies from one metal surface to another and for different ion compositions. U(PZC) is often approximated to be 0 on the reversible hydrogen electrode (RHE) scale. Therefore, for an electric field of 0.5 V/Å within a Helmholtz layer of 3 Å, the electrode potential is 1.5 V_{RHE}. However, such an approximation cannot capture the impact of the adsorbate in shifting the metal work function, which especially needs to be improved when an adsorbate/electrode system has a large dipole moment. On the other hand, adjusting the number of electrons within the unit cell and adding a compensating homogeneous background charge in the double reference method [39] can change the surface potential and generate an electric field at the electrode-electrolyte interface [38]. The electric field is related to the electrode potential (V_{NHE}) by:

$$V_{NHE} = \phi/e - 4.6 \quad (4)$$

where ϕ is the calculated work function referenced to vacuum, e is the charge of an electron and 4.6 V is the estimated potential of the vacuum of the normal hydrogen electrode (NHE) scale in fuel cells [40]. In addition, to generate electrode potentials above 1.1 V (or below 0.5 V), the top of the metal slab is positively charged (or negative charged) by selectively adding (subtracting) a number of electrons to the system. This relates to the calculated system in the presence of a simulated positive field (a simulated negative field) in the NS method since such a system includes a positively charged (a negatively charged) metal slab.

In this present paper, by using the NS method, we will show the significance of the electric field effects on the energetics of the MSR-on-Ni reaction. Several researchers have proposed [41–43] that surface OH and O species can be key intermediates that react with the surface CH_x species. Thus we examined mechanisms for the overall MSR reaction that include both CH_xOH and CH_xO species (given in Fig. 1). To identify the relative equilibrium stabilities of the MSR intermediates under realistic conditions, we also provide a first-principles-based phase diagram for the CH_xOH and CH_xO species as a function of the hydrogen chemical potential and the applied electric field. Based on our previous studies, we also anticipate that many of the results obtained here on a Ni(111) flat surface will be applicable to stepped surfaces as well [29–31]. The paper ends with the significant findings on the field effects on the heterogeneous reaction and an outlook on the remaining challenges of field-dependent heterogeneous reactions.

2. Methods

Our DFT calculations were performed with the Vienna *Ab Initio* Simulation Package (VASP). For adsorbates/late transition metal system, it was recently found in a benchmarking study that the Perdew-Wang 91 functional is of comparable accuracy to the PBE, PBEsol and RPBE functionals when examining a large variety of adsorption systems [44]. As a result, for all calculations we used the Generalized Gradient Approximation with the PW91 exchange correlation functional (GGA-PW91) [45–47]. The projector-augmented wave method was applied to solve the Kohn-Sham equations [48]. The choices for the k-point mesh (4 × 4 × 1), the lattice constant of Ni (3.521 Å), the plane-wave energy cutoff (400 eV), the vacuum size (11 Å) [31,49], and four-layer Ni slab was tested in our previous work [29–31]. An increase in the energy cut-

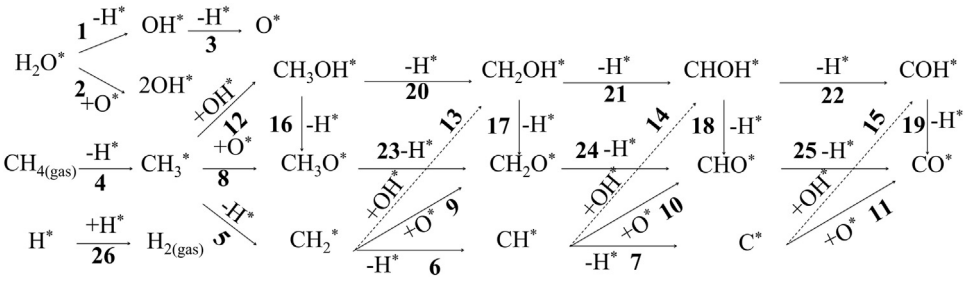

Fig. 1. Proposed mechanisms of methane steam reforming (MSR) on Ni(111).

off to 450 eV and the *k*-point mesh to 6 × 6 × 1 kpoints was found to change the adsorption energies of CH_x by less than 0.02 eV [29]. The adsorption energies differences between our 4-layer and 5-layer Ni slab models were all less than 0.01 eV [31]. Therefore, all the energies reported in this manuscript are estimated with an accuracy of 0.01 eV. Additionally, we considered the influence of van der Waals corrections (optB88-vdW) on the physisorption of a CH_4 molecule over a Ni(1 1 1) surface in the presence of an electric field. The inclusion of the van der Waals forces strengthened the adsorption energy methane by ~0.13 eV and shifted the dissociation of methane to form CH_3 and H by only ~0.02 eV regardless of the electric field strength (see Fig. S10). Since these changes are not significant, we used PW91 functional in our DFT calculations.

Adsorption energies (E_{ad}) of isolated intermediates on a Ni(111) surface were calculated from Eq. (5) and the reaction energies (ΔH_{rxn}) of the $A + B \rightarrow C + D$ elementary reactions were calculated by Eq. (6):

$$E_{ad}(F) = E_{A/slab}(F) - E_{slab}(F) - E_A(F) \quad (5)$$

$$\Delta H_{rxn}(F) = E_{C+D/slab}(F) - E_{A+B/slab}(F) \quad (6)$$

where $E_{A/slab}$, E_{slab}, and E_A are the total energies of molecule **A** adsorbed on the slab, the clean slab, gas phase molecule **A**, respectively. Finally, *F* is the applied field strength. Endothermic reactions are accompanied by positive values of ΔH_{rxn}.

3. Results and discussion

3.1. Electric field effects on the adsorption energy of MSR intermediates

To better understand the field effects on the MSR reaction, we simulate the influence of an electric field on the order of −1 V/Å to 1 V/Å on this system. With such a strong applied electric field, the metal/adsorbate system interacts with a field that can stabilize or destabilize the adsorbate based on both the surface dipole moment as well as the polarizability it induces to the interface, and can subsequently alter the mechanisms of the heterogeneous reactions. The field effects on the adsorption energies (E_{ad}) of the MSR species at their most favorable configurations (Fig. 2) are given in Table 1 and Fig. 3. The electronic structures with tunable electric fields for H_2O, OH, O and CH_x (x = 0–3) species have already been discussed in our previous work [29,31]. The details regarding to the adsorption structures of various MSR-involved species over Ni(111) in the absence of an electric field are given in the ESI Section 1.

3.1.1. Electric field effects on the adsorption of CH_xO species

Fig. 3(a) shows the adsorption energies of the most favorable CH_xO (x = 0–3) configurations as a function of the applied electric field strength. Applied electric fields affect the adsorption energies of CH_3O, CH_2O and CO in a similar way, in which their adsorption energies are monotonically weakened as the field strength is increased from −1 V/Å to 1 V/Å. In contrast to the other CH_xO species, both positive and negative fields decrease the adsorption strength of CHO. Comparing the field effects on all of the CH_xO species, we find that the CH_2O species has the largest influence: the adsorption energy of CH_2O differs by up to 0.6 eV for field values ranging from −1 V/Å to 1 V/Å. Since the E_{ad} value of a CH_2O molecule is only −0.45 eV in the presence of a positive field of 1 V/Å, CH_2O likely desorbs from the surface as a byproduct rather than adsorbing as a MSR reaction intermediate. Importantly, since the adsorption energy of CO is ~0.5 eV smaller at a field value of 1 V/Å as compared to when a field strength of −1 V/Å is applied, we also conclude that a strong positive electric field can assist in the desorption of the CO product from a flat Ni surface.

3.1.2. Electric field effects on the adsorption of the CH_xOH species

The electric field effects on the adsorption of the CH_xOH (x = 0–3) species on Ni(111) are shown in Fig. 3(b). The field effects on the adsorption of CH_2OH and CH_3OH are similar to the ones of H_2O on Ni(111) from our previous work [31], the adsorption energies of CH_3OH strengthen from −0.05 eV to −0.47 eV and the adsorption geometries of the OH segment of CH_3OH alters from a H-down structure to H-up structure as we increase the field value from -1 V/Å to 1 V/Å (Fig. 4).

3.1.3. Electric field effects on the adsorption of MSR-involved species

In combination with our previous work [29,31] along with the results in the present investigation on the adsorption of CH_x (x = 0 ~ 3) and H_xO (x = 0 ~ 2) species as a function of the field strength, we conclude several key points here. A positive electric field strengthens the adsorption of reactants ($CH_4 + H_2O$) on Ni(111) and facilitates the desorption of products ($CO + H_2$). The electric field effects on the adsorption energies of CH_xO and CH_xOH are more significant than those on the CH_x species [29]. Interestingly, the chemisorption species, such as CH_3O, CHO, CHOH or COH, have a similar dependence on the electric field, in which a negative electric field further stabilizes their adsorption. Conversely, the physisorbed byproducts, such as CH_3OH, CH_2O are further destabilized on the surface with a negative electric field. However, such an influence of an electric field on the adsorption of methanol is also of interest since it is a more desirable product than syngas for other industrial applications [50].

3.2. Electronic properties analysis for electric field effects

3.2.1. Adsorption geometries

Table 1 shows how an electric field, on the order of −1 V/Å to 1 V/Å, influences the adsorption geometries of MSR intermediates on a Ni(111) surface. As compared to the geometries in the absence of a field, the O atoms of all CH_xOH (x = 0 ~ 3) and CH_xO (x = 0 ~ 3) species are farther away from the surface when a negative electric field is applied, while the O atoms of these species are closer toward

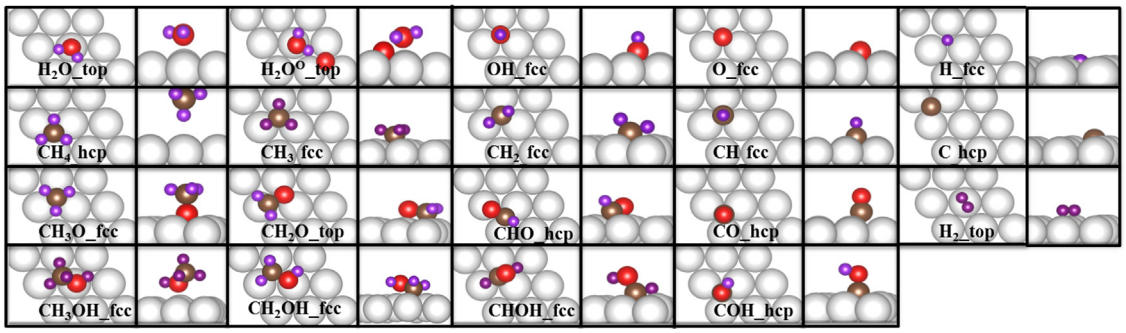

Fig. 2. The top and side views of the most favorable adsorption structures of all MSR-involved possible intermediates on a Ni(111) surface. For the CH_xOH_y species, the site labeling refers to the surface carbon position.

Table 1
Summary of electric field effects on the adsorption of possible MSR intermediates at their most favorable adsorption sites.

Species	Site	E_{ad} (eV)	$d_{C(O)-H}$ (Å)	d_{C-O} (Å)	$d_{Ni-O(C)}$ (Å)
CH_4	hcp	−0.00/−0.04/−0.09	1.10/1.10/1.10	–	4.06/4.05/4.04
CH_3O	fcc	−2.94/−2.84/−2.67	1.10/1.10/1.10	1.42/1.44/1.46	1.99/1.98/1.96
CH_2O	top	−0.45/−0.80/−1.11	1.10/1.10/1.10	1.39/1.38/1.37	2.01/1.99/1.98
CHO	hcp	−2.28/−2.35/−2.05	1.11/1.11/1.11	1.30/1.29/1.28	1.95/1.96/1.97
CO	hcp	−2.11/−1.93/−1.69	–	1.21/1.19/1.18	1.94/1.95/1.96
CH_3OH	fcc	−0.05/−0.31/−0.47	1.10/1.10/1.10	1.43/1.45/1.46	4.02/2.15/2.08
CH_2OH	fcc	−1.12/−1.70/−1.34	1.11/1.10/1.12	1.45/1.46/1.45	2.43/2.14/2.07
CHOH	fcc	−3.29/−3.05/−2.74	1.16/1.18/1.21	1.40/1.37/1.35	1.97/1.96/1.96
COH	hcp	−4.54/−4.53/−4.19	0.98/0.98/0.99	1.37/1.34/1.31	1.85/1.86/1.87
H_2	top	−0.14/−0.27/−0.38	–	–	–

Note: The numbers in each column from left to right represent the adsorption of possible intermediates in the presence of a negative electric field, in the absence of an electric field, and for a positive electric field value, respectively. For the $d_{C(O)-H}$ column, we only give the O—H distance for a COH molecule, while the others represent the C—H distance. For the $d_{Ni-O(C)}$ column, we give the Ni—O distance for CH_3O, CH_2O, CH_3OH molecules, while the others represent the Ni—C distance.

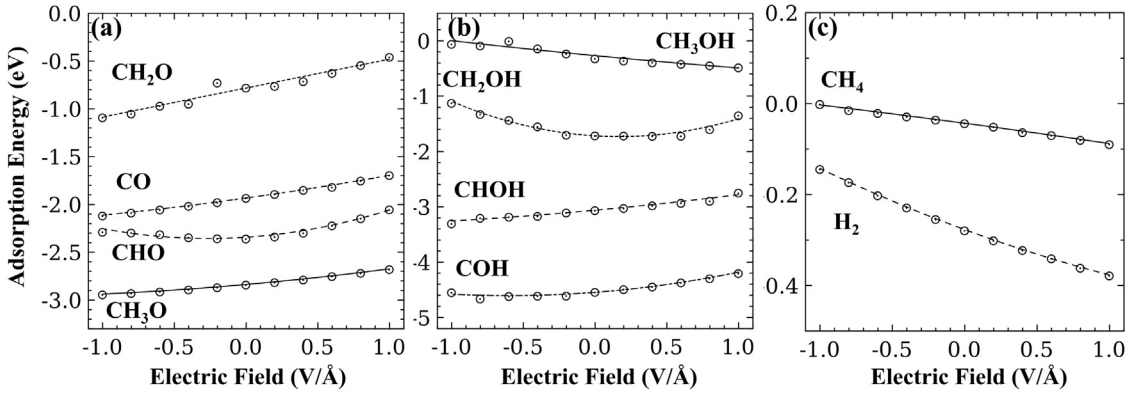

Fig. 3. The field-dependent trendlines of the MSR-involved species as the function of an applied electric field, including (a) the CH_xO species (x = 0~3), (b) the CH_xOH species (x = 0~3) and (c) the CH_4 and H_2 species. The dots represent their adsorption energies under a particular electric field strength ranging from −1 V/Å to 1 V/Å at an interval of 0.2 V/Å.

the surface when applying a positive electric field. This is similar to our previous work on the electric field effects on the adsorption geometries of H_2O on Ni(111) [31]. The reason for these effects is that the O atoms of all CH_xOH (x = 0–3) and CH_xO (x = 0–3) species are negatively charged, which is attracted to the positively charged metal surface in the presence of a positive electric field. On the other hand, a negative electric field direction points toward the surface (as shown in Fig. 4) and polarizes the top of the Ni surface with a partial negative charge and consequently repels the negatively charged O atoms. This explanation also can be used to better understand the adsorption of the CH_x species when the C atom is bonded to the surface. For example, the C atom of a CH_4 molecule is partially negatively charged. As a result, the C atom is closer to the surface when a positive electric field is applied and is further away from the surface when we apply a negative electric field. Conversely, the C atom in a CO and a COH molecule is partially positively charged and an electric field has the opposite effect on the Ni-C distance as compared to its effect on the Ni-C distance on a CH_x molecule.

3.2.2. *Effective dipole moments and effective polarizability analysis*

The effect of a simulated field on the E_{ad} values of the species involved in the MSR reaction can be given in terms of a Taylor series expansion [33,34,51–55]:

$$E_{ad} = E_{ad0} - \Delta d_{F=0}F - \frac{1}{2}\Delta\alpha_{F=0}F^2 + \ldots \quad (7)$$

where all the Taylor coefficients, E_{ad0}, $\Delta d_{F=0}$ (effective dipole moment), and $\Delta\alpha_{F=0}$ (effective polarizability [53]) are evaluated at $F = 0$ V/Å. More details on how to derive this equation can be

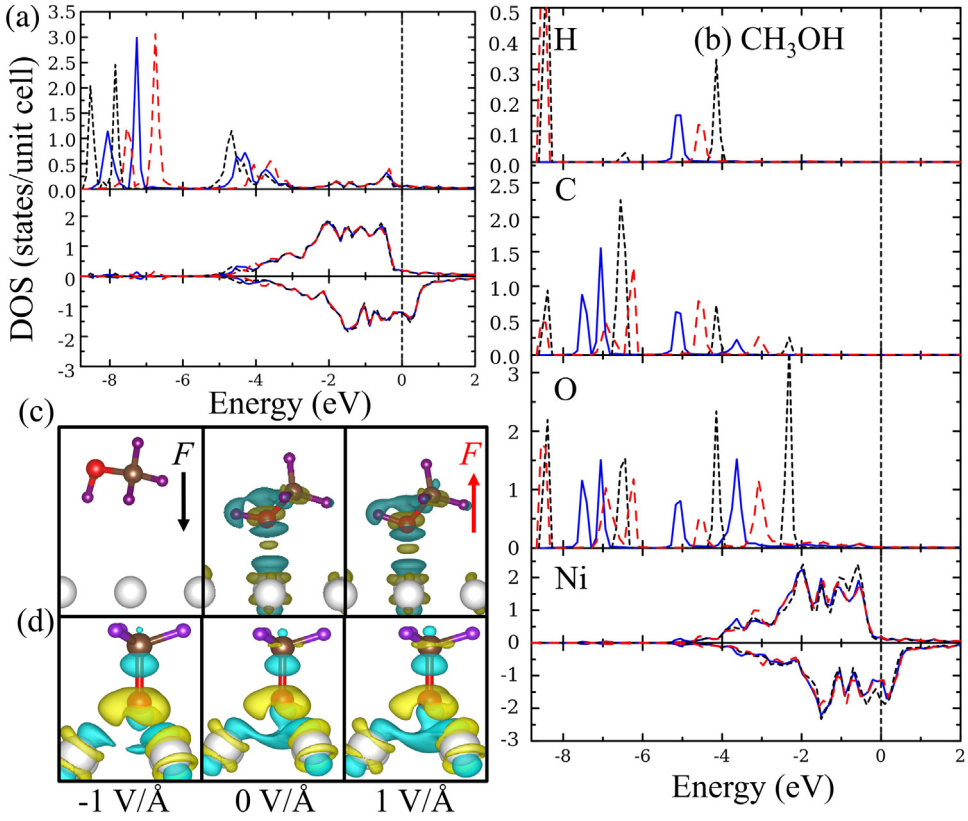

Fig. 4. Projected density of states (DOS) of CH_3O (a) and CH_3OH (b) on the Ni(111) surface. Parts (c) and (d) correspond to their differential charge densities in the presence and the absence of an electric field. Red, blue and black lines in part (a) and (b) represent the DOS with a positive field, no fields and a negative field, respectively. The energy scale of the DOS are relative to the Fermi energy, as indicated by the vertical black dotted line. The isosurface level of the differential charge densities of CH_3O (c) and CH_3OH (d) are 0.003 and 0.007 e/bohr^3. The yellow or blue areas represent a gain or loss of electrons. (For interpretation of the references to colour in this figure legend, the reader is referred to the web version of this article.)

found in our previous work [31]. The values of $\Delta d_{F=0}$ and $\Delta\alpha_{F=0}$ of all MSR-involved species are the first and second derivatives of field-dependent energies (Fig. 3), which are summarized in Table 2.

From Fig. 3, it is clear that the adsorption of CH_2O has the most significant field effect, which correlates well with the fact that its effective dipole moment in Table 2 is the largest. Fig. 3(a) shows that the CH_3O, CH_2O and CO species have similar electric field effect trends. A positive electric field weakens their adsorption energies and a negative electric field strengthens them. This also correlates well with the fact that the signs of their effective dipole moments are all positive. The sign of the dipole moments of all weakly adsorbed species (CH_3OH, CH_4, H_2O and H_2) are the same as well, and thus the field has similar influences on the weakly adsorbed species. Therefore, we conclude that the field influence on the adsorption energy mainly depends on the magnitude of their corresponding effective dipole moments. We also find that the magnitude of $\Delta d_{F=0}$ for all the MSR-involved species obeys the following order:$CH_xO > CH_xOH > H_xO > CH_x$.

3.2.3. Electronic properties analysis

In Sections 3.1 and 3.2.2, we found that the presence of an electric field gave similar trends for the strongly adsorbed species (e.g. CH_3O) and had opposite trends for the weakly adsorbed species (e.g. CH_3OH). To give a qualitative analysis on the electric field effects on the electronic interactions between the adsorbates and the metal surface, we present both the projected density of states (PDOS) and a differential charge density analysis of the isolated adsorbed MSR intermediates (CH_xO and CH_xOH groups) on the Ni(1 1 1) surface. Since the electronic properties of the strongly adsorbed species (CH_2O, CHO, CO, CHOH and COH) are similar to CH_3O and the weaker adsorbed species (CH_2OH) have similar trends as that found for CH_3OH, we only show the DOS and differential charge density analysis of CH_3O and CH_3OH in Fig. 4. More details regarding to the DOS and the differential charge density analysis of the other CH_xO and CH_xOH species are given in Fig. S11-S13. Furthermore, the differential charge density shows that an adsorbed CH_3OH molecule has no charge transfer with the metal surface in the presence of a negative field but has a significant amount of charge transfer for positive field values, which corresponds well with the monotonically increasing adsorption energy of CH_3OH with increasing field strength. Similarly, the O atom gains slightly more electrons from the metal surface when examining the differential charge density of CH_3O in the presence of a negative field than it does in the presence of a positive field or in the absence of a field. This also correlates well with its adsorption energy since it is stronger for negative field values than it is in the absence of a field or for positive field strengths.

3.2.4. Bader charge analysis

To give a quantitative analysis on the electric field effects on the charge transfer at the interface of the adsorbate/metal system, we present in Table 3 a Bader charge summary [56]. When we calculated the Bader charge analysis, we applied a fast Fourier transform (FFT) grid that was twice as dense as compared to the standard FFT grid so as to ensure that the Bader charge results were fully converged. In the absence of a field, the CH_3OH, CH_4, and H_2 molecules have almost no electronic interactions with the metal surfaces. This correlates well with the fact that these species adsorb very weakly on the Ni surface. These weakly adsorbed species have similar field effects on their charges. With a positive electric field, the

Table 2
Summary of the effective dipole moments (in units of eV·Å/V) and effective polarizabilities (in units of eV·Å^2/V^2) for the MSR-involved species on Ni(111).

IS	$\Delta d_{F=0}$	$\Delta\alpha_{F=0}$	FS	$\Delta d_{F=0}$	$\Delta\alpha_{F=0}$
H_2O	**0.25**	**−0.15**	OH, H	0.08	−0.52
OH	−0.09	−0.05	**O, H**	**−0.34**	**−0.06**
O	−0.08	−0.20			
H_2O, O	0.21	−0.40	OH, OH	−0.13	0.19
CH_4	0.04	0.00	**CH_3, H**	**0.14**	**−0.09**
CH_3	**0.19**	**−0.02**	CH_2, H	−0.06	−0.02
CH_2	0.14	−0.02	CH, H	−0.07	−0.01
CH	0.08	−0.19	C, H	−0.15	−0.05
C	−0.07	−0.18			
CH_3O	−0.13	−0.06	**CH_3, O**	**0.19**	**−0.11**
			CH_2O, H	−0.18	−0.06
CH_2O	**0.30**	**0.00**	CH_2, O	−0.04	0.05
			CHO, H	−0.09	−0.02
CHO	−0.10	−0.38	CH, O	−0.01	0.06
			CO, H	**−0.22**	**−0.01**
CO	−0.21	−0.06	C, O	−0.04	0.09
CH_3OH	**0.25**	**−0.05**	CH_3, OH	−0.13	0.52
			CH_2OH, H	−0.03	−0.41
			CH_3O, H	0.02	−0.24
CH_2OH	0.16	−0.93	CH_2, OH	0.12	−0.07
			CHOH, H	**−0.17**	**−0.03**
			CH_2O, H	**−0.14**	**−0.07**
CHOH	−0.24	−0.08	**CH, OH**	**0.23**	**−0.09**
			COH, H	0.11	−0.02
			CHO, H	−0.06	−0.08
COH	−0.20	−0.33	C, OH	−0.01	0.14
			CO, H	**−0.37**	**−0.11**
H	−0.01	−0.03	H, H	0.14	0.04
H_2	0.12	−0.07			

Note: 'H_2O, O' represents the adsorption of a H_2O molecule with a pre-adsorbed O atom.

adsorbates gain slightly more charges from the surface than the scenarios in which there are no fields, which correlates well with the fact that a positive field only alters their adsorption strength slightly. For negative field values, the surface becomes partially negatively charged and this repels the negatively charged C atom of the adsorbed species (e.g. CH_3OH, CH_4) and consequently leads to a much weaker adsorption.

Similar electric field effects are found for the other MSR intermediates, including CH_xO (x = 0–3) and CH_xOH (x = 0–2). In the absence of a field, the O atoms of the above species gain ~1 e from both the metal slab and the CH_x segment, and become negatively charged. The H atom, which is bonded to the O atom of CH_xOH species, loses ~0.85 e and becomes positively charged. Overall, these intermediates gain a net charge from the Ni surface. For positive field values, the transferred charge between each adsorbate and the metal surface decreases, while a negative field value has the opposite effect. By combining this information with the bond strength of the MSR intermediates in Fig. 3, we find that the stronger bond strength of the intermediates correlates well with the amount of charge transferred between the metal surface and the adsorbates. For example, upon adsorption of a CH_2O molecule in the presence of an applied field the charge transferred between Ni surface and CH_2O adsorbate decreases by ~0.3 e as one increases the field value from −1 V/Å to 1 V/Å. This mirrors the fact that the adsorption energy of CH_2O is monotonically weakened as one varies the field strength from −1 V/Å to 1 V/Å.

The adsorption of CH_2OH is an exception, since the adsorption energy of a CH_2OH molecule becomes weaker with a negative field but the amount of charge transferred increases in such an environment. As shown in Fig. S14, combining the Bader charge analysis and the differential charge density, it shows that the presence of a positive electric field polarizes the surface with a partial positive charge, which has a Coulomb attraction with the partial negative charge of the O atom in the CH_2OH molecule and further strengthens the adsorption of this molecule. On the other hand, a negative electric field polarizes the surface with partial negative charge, which has a Coulomb repulsion with the partial negative charge of the O atom in the CH_2OH molecule and further weakens the adsorption of this molecule. This corresponds well with our calculations where the adsorption energy of a CH_2OH molecule over a Ni(111) surface with a negative field is much weaker than the ones with a positive field based on the Coulomb forces. In addition, with a positive electric field, two H atoms (bonded to the C atom) are partially positively charged, which form two internal dipole moments with the bonded C atom (see Fig. S14). The direction of the dipole moments of the C—H bonds aligns with a positive electric field, which further stabilizes the system. On the other hand, the direction of the dipole moments of the C—H bonds is not aligned with the negative electric field. As such, a negative electric field leads the majority of the transferred charges to be from the metal slab to the H atoms (bonded to the C atoms). Consequently, there is no internal dipole moment between the C and H atoms. This leads to a weaker adsorption of the molecule as compared to when a positive field is present even though the total amount of transferred charges (0.34 e) with a negative field is larger than that in the presence of a positive electric field (0.13 e).

Overall, an electric field notably affects the adsorption of the MSR-involved species on a Ni(111) surface and consequently changes the underlying energy landscape involved in the such a reaction. The field effects can be rationalized through an analysis of the effective dipole moments, the electronic geometries, the DOS, and differential charge densities of the adsorbed species. Their transferred charges are quantified with a Bader charge analysis between the adsorbate and metal surface. This further enhances our understanding of the underlying interactions between the MSR-involved species and a Ni catalyst surface in the presence of an electric field.

3.3. MSR reaction energies in the presence of the electric fields

The reaction energy (ΔH_{rxn}) is a key element needed to determine the underlying reaction pathway. From Sections 3.1 and 3.2, it is clear that the presence of a field significantly changes the electronic interactions between the intermediates and the metal surface. Here, we examine how an electric field influences the reaction energies of each possible elementary reaction that could be involved in the underlying MSR reaction (Fig. 5). Co-adsorption occurs for either the initial state (IS), in the case of synthetic elementary reaction steps; or the final state (FS), in the case of dissociative elementary reaction steps. Such information can also help estimate the field-dependent activation energy of each elementary reaction and determine the most favorable pathway in the presence of an electric field if one constructs a Brønsted-Evans-Polanyi (BEP) relation [57–60] in which the activation energy is linearly correlated with ΔH_{rxn} [61,62]. Details with respect to the most favorable co-adsorption configurations of the FS and IS for each possible elementary reaction in the absence of an electric field are shown in Fig. S9 and their corresponding reaction energies with no fields (calculated by Eq. (6)) are summarized in Table S4.

3.3.1. Dehydrogenation of CH_x and H_xO species with different electric fields

As Fig. 1 shows, the MSR reaction starts with the dehydrogenation of the CH_4 and the H_2O reactants. From Section 3.1, we know that CH_4 is very weakly adsorbed on the surface, and it prefers to dissociate to form CH_3 with H. The reaction energy for $CH_4 \rightarrow CH_3 + H$ is nearly energy neutral. As we vary the field value from −1 V/Å to 1 V/Å, the reaction energy decreases from 0.24 eV to

Table 3
Bader charge analysis of the MSR intermediates as a function of an electric field.

Species	Δe = Ni(e)-360e	Δe = O(e)-6e	Δe = C(e)-4e	Δe = nH(e)-ne
CH_4	−0.05/−0.02/0.01	–	0.17/0.13/0.13	−0.12/−0.11/−0.14
CH_3O	−0.59/−0.50/−0.41	1.09/1.06/1.03	−0.41/−0.35/−0.30	−0.09/−0.22/−0.32
CH_2O	−0.62/−0.49/−0.36	1.01/0.99/0.97	−0.30/−0.32/−0.33	−0.09/−0.18/−0.28
CHO	−0.55/−0.43/−0.31	1.04/0.99/0.95	−0.41/−0.43/−0.45	−0.07/−0.13/−0.20
CO	−0.49/−0.38/−0.28	1.07/1.02/0.96	−0.58/−0.64/−0.68	–
CH_3OH	−0.07/0.00/0.08	1.14/1.13/1.12	−0.39/−0.31/−0.29	−0.68/−0.82/−0.91
CH_2OH	−0.34/−0.23/−0.13	1.12/1.07/1.06	−0.08/−0.04/−0.04	−0.71/−0.80/−0.89
CHOH	−0.34/−0.24/−0.11	1.05/1.07/1.17	−0.22/−0.20/−0.27	−0.60/−0.63/−0.68
COH	−0.39/−0.27/−0.15	1.14/1.10/1.13	−0.15/−0.21/−0.31	−0.60/−0.62/−0.67
H_2	−0.07/−0.02/0.04	–	–	0.07/0.02/−0.04

Note: 1. The number in each column from left to right represents the charge differences of the species in the presence of a negative electric field, in the absence of a field, and a positive electric field, respectively.
2. The 2nd column 'Δe = Ni(e)-360e' represents the charge gain or loss of the metal surface for each intermediate since each Ni atom has 10 e and we have 36 Ni atoms in each metal slab. This number also equals the charge loss or gain of the corresponding adsorbates.
3.The 3rd, 4th and 5th column show the charge gain or loss for the O, C and H atoms in each species.
4. A positive sign means that the system gains a charge, while the negative sign stands for a charge loss.

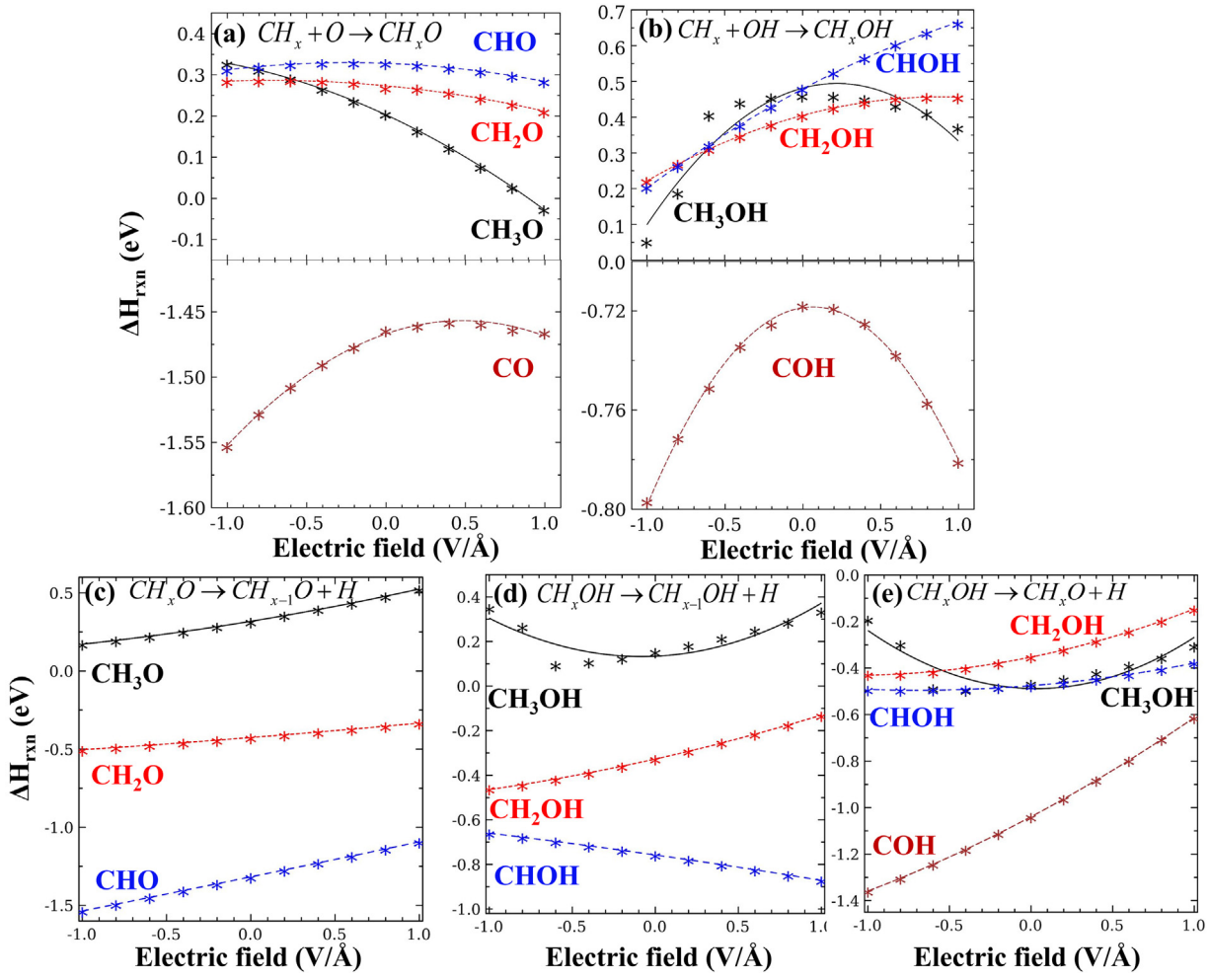

Fig. 5. The field-dependent reaction energy trendlines of different elementary reactions proposed in Fig. 1 in the presence of different electric fields on a Ni(111) surface. The dots represent their adsorption energies under a particular electric field strength ranging from −1 V/Å to 1 V/Å at an interval of 0.2 V/Å.

−0.03 eV. This has an opposite field effect as compared to the dehydrogenation reaction energies of the other CH_x groups (x = 1–3). Similarly, the changes of the dipole moments (Table 2) associated with the dehydrogenation of the CH_x (x = 1–3) species are of opposite sign to those involved for the dehydrogenation of CH_4. From our previous work [29], we know that a positive electric field doesn't largely alter the dehydrogenation of the CH_3 and the CH_2 species, but that it does alter the $CH \rightarrow C + H$ reaction by raising its reaction barrier, which suppresses pure carbon formation. Early investigations [31] also showed that a negative electric field can accelerate the dehydrogenation of H_2O to form surface OH and O species, while a positive electric field can hinder its dehydrogenation. This fundamental information can guide us toward the design of new MSR catalysts that prevent coking and enhance the efficient utilization of steam: it is better to perform water dehydrogenation in the presence of a negative electric field in one step, and methane

dissociation in the presence of a positive electric field as the other step. In this way, sufficient surface OH and O species can be produced, which can oxidize the CH_x (x = 1–3) groups to form CH_xOH and CH_xO species and further prevent coking.

3.3.2. Electric field effects on the formation of CH_xO and CH_xOH species

CH_x (x = 0–3) segments can get oxidized with OH and O, which can then form CH_xO and CH_xOH species on Ni(111). Except for the formation of CO and COH, the formation energies of other CH_xO (~0.3 eV) and CH_xOH (~0.42 eV) species are all endothermic. Additionally, the formation energies of CHO and CHOH are much smaller than those involved in the dissociation of a CH molecule. As a result, an CH intermediate seems to prefer to be oxidized by surface OH or O species rather than dissociating to a pure C atom. The formation of COH and CO from pure C atoms on a Ni(111) surface are both exothermic, which suggests that even though pure carbon atoms may form on Ni(111), sufficient surface O or OH segments can prevent the formation of coke as well.

After one applies an electric field to the most favorable co-adsorption configurations involving the CH_x and the O species to the corresponding $CH_x + O \rightarrow CH_xO$ reactions, we find that the reaction involving the formation of CH_3O has the most significant field effect (Fig. 5(a)). This can also be checked in Table 2, wherein the formation of CH_3O has the largest effective dipole moment with a value of 0.19 eV·Å/V. In the presence of a field of 1 V/Å, the $CH_3 + O \rightarrow CH_3O$ reaction is nearly energy neutral, while the reaction energy monotonically increases by ~0.4 eV as we decrease the electric field values from 1 V/Å to −1 V/Å. For the reactions involving the oxidation of CH_x with hydroxyl group, the formation energy of CHOH has the largest field effect. The $CH + OH \rightarrow CHOH$ reaction energy monotonically increases by ~0.5 eV as we increase the electric field strength from −1 V/Å to 1 V/Å (Fig. 5(b)). Therefore, based on the BEP linearly correlations, CH_x species are easier to be oxidized by a hydroxyl group than that by a surface oxygen species in the presence of a negative electric field, while a positive electric field has an opposite effect. This indicates that with different electric fields, the overall MSR reaction mechanism can be modified.

3.3.3. Dehydrogenation of CH_xO and CH_xOH species in the presence of a field

Fig. 5(c) shows how an electric field has the similar effects on breaking the C—H bond for all the CH_xO species, in which a negative field drives the ΔH_{rxn} values for its dehydrogenation to $CH_{x-1}O$ to much smaller values as compared to when a positive electric field is applied. Comparing the $\Delta d_{F=0}$ values for the CH_xO dehydrogenation reactions (Table 2) one can see that the CHO dehydrogenation has the greatest field effect: its reaction energy increases by ~0.5 eV when one increases the field value from −1 V/Å to 1 V/Å. Interestingly, since the dehydrogenation of the CH_xO species has C—H cleavage, the field effects on the reaction energies of its dehydrogenation to $CH_{x-1}O$ reactions are similar to the ones for the methyl dehydrogenation from our previous work [29].

Dehydrogenation of CH_xOH can either break the C—H bond (Fig. 5(d)) or break the O—H bond (Fig. 5(e)). For methanol, the breaking of the C—H bond via the $CH_3OH \rightarrow CH_3O + H$ reaction is endothermic with a ΔH_{rxn} value of 0.15 eV. The reaction energy increases by 0.24 eV when one increases the field value from −1 V/Å to 1 V/Å. On the other hand, the breaking the O—H bond in a methanol molecule to form a CH_3O is exothermic with a ΔH_{rxn} value of −0.47 eV. The electric field effects on this reaction are similar to that on the $CH_3OH \rightarrow CH_2OH + H$ reaction. Since the $CH_3OH \rightarrow CH_3O + H$ reaction is exothermic and the $CH_3OH \rightarrow CH_2OH + H$ reaction is endothermic, we conclude that it is energetically more favorable to break the O—H bond in a CH_3OH molecule. In particular, a negative electric field of −0.6 V/Å further makes the O—H bond breaking more exothermic. A similar analysis can be applied for the C—H and O—H bond breaking of CH_2OH and CHOH. The O—H bond breaking of CH_2OH is more energetically favorable than its counterpart C—H bond breaking in the presence of a field value of −1 V/Å. Moreover, the C—H bond breaking of CHOH is ~0.3 eV more exothermic and has a larger field influence than the breaking of the O—H bond. Furthermore, O—H bond breaking of a COH molecule is the most exothermic reaction among all the dehydrogenation reactions of the CH_xOH species, with a ΔH_{rxn} value of −1.04 eV. Additionally, the $COH \rightarrow CO + H$ reaction has the greatest electric field effect as well, in which the reaction energy of the $COH \rightarrow CO + H$ reaction monotonically increases from −1.36 eV to −0.61 eV as we increase a field value from −1 V/Å to 1 V/Å.

Overall, for the formation of CH_xO or CH_xOH, a positive electric field facilitates the oxygen oxidation of the CH_x species, while a negative electric field accelerates the hydroxyl oxidation of the CH_x species. We also examined the C—H or O—H bond breaking of these species and found that these bond breaking reaction energies are much smaller than their formation energies and also had larger field effects. Except for CHOH, the dehydrogenation of the other CH_xO and CH_xOH species has similar field effects: a negative electric field lowers the ΔH_{rxn} values and a positive field enlarges the ΔH_{rxn} values. Comparing the dehydrogenation reactions of CH_xO and CH_xOH, the reactions having larger field dependences are in following order $COH \rightarrow CO + H > CHO \rightarrow CO + H > CH_3O \rightarrow CH_2O + H$.

3.4. Phase diagram from first principles of MSR intermediates

3.4.1. Phase diagram

The change of Gibbs free energy of adsorption (ΔG) as a function of the hydrogen chemical potential ($\Delta\mu_H$) and the electric field strength (F) can provide us with a connection between our DFT calculations and the relative equilibrium stabilities of the possible MSR intermediates under various experimental conditions [63–66]. The following paragraph explains how we define ΔG based on our calculations from first principles.

The formation of the CH_xOH_y (y = 0 or 1), CH_x and OH_y species on Ni(111) under MSR conditions is shown in Eqs. (8)–(10) and the binding energy ($E_b{}^{CH_xOH_y{}^*}$, $E_b{}^{CH_x{}^*}$, $E_b{}^{OH_y{}^*}$) is defined in Eqs. (11)–(13).

$$CH_4 + H_2O + * \rightarrow CH_xOH_y{}^* + \frac{6-x-y}{2}H_2 \quad (8)$$

$$CH_4 + * \rightarrow CH_x{}^* + \frac{4-x}{2}H_2 \quad (9)$$

$$H_2O + * \rightarrow OH_y{}^* + \frac{2-y}{2}H_2 \quad (10)$$

$$E_b{}^{CH_xOH_y{}^*} = E_{CH_xOH_y{}^*} + \frac{6-x-y}{2}E_{H_2} - E_* - E_{CH_4} - E_{H_2O} \quad (11)$$

$$E_b{}^{CH_x{}^*} = E_{CH_x{}^*} + \frac{4-x}{2}E_{H_2} - E_* - E_{CH_4} \quad (12)$$

$$E_b{}^{OH_y{}^*} = E_{OH_y{}^*} + \frac{2-y}{2}E_{H_2} - E_* - E_{H_2O} \quad (13)$$

where $E_{CH_xOH_y{}^*}$, $E_{CH_x{}^*}$, $E_{OH_y{}^*}$ are the total energies of the isolated intermediates (CH_xOH_y, CH_x, OH_y) on the top of a Ni(111) surface and '*' stands for a clean Ni(111) slab, while E_{H_2}, E_{CH_4}, and E_{H_2O} represent the gas phase energies of H_2, CH_4 and H_2O, respectively. ΔG is then obtained by Eqs. (14)-(16) [64,66].

$$\Delta G = E_b{}^{CH_xOH_y{}^*} + (6-x-y)\Delta\mu_H - \Delta\mu_{CH_4} - \Delta\mu_{H_2O} \quad (14)$$

$$\Delta G = E_b{}^{CH_x{}^*} + (4-x)\Delta\mu_H - \Delta\mu_{CH_4} \quad (15)$$

$$\Delta G = E_b{}^{OH_y{}^*} + (2-y)\Delta\mu_H - \Delta\mu_{H_2O} \quad (16)$$

where $\Delta\mu_H$ is defined as $\Delta\mu_H = \mu_H - \frac{1}{2}E_{(H_2)}$ since we take H_2 as the hydrogen reference. Similarly, we can also get $\Delta\mu_{CH4}$ and $\Delta\mu_{H2O}$. At 0 K and standard pressure conditions, we define $\mu_H(0K, {p_0}^{H_2}) = \frac{1}{2}E_{(H_2)} \equiv 0$.

From the above paragraphs, we have completely described how we obtain ΔG from our DFT calculations as a function of $\Delta\mu_H$. The next step is to relate the $\Delta\mu_H$ to our realistic temperature and hydrogen partial pressure. Via the formula for a pure ideal gas (i.e. H_2) (Eq. (17)), we can include the effect of pressure and temperature on $\Delta\mu_H$. Here we assume that $2H \rightleftarrows H_2$ is at equilibrium.

$$\Delta\mu_H(T, {p}^{H_2}) = \Delta\mu_H(T, {p_0}^{H_2}) + \frac{1}{2}k_BT\ln\frac{p}{p_0} \quad (17)$$

where ${p}^{H_2}$ and ${p_0}^{H_2}$ represent the practical partial pressure and standard partial pressure of H_2, and k_B is the Boltzmann's constant. This equation provides us with a description of how the hydrogen chemical potential is altered by the pressure at a certain temperature. Additionally, we also have to figure out how to obtain the value of $\Delta\mu_H(T, {p_0}^{H_2})$. With respect to $\mu_H(0K, {p_0}^{H_2})$, $\mu_H(T, {p_0}^{H_2})$ is given in Eq. (18). The values of enthalpy H and entropy S at a certain temperature and standard pressure can be found in Thermodynamic Tables [67]. Since $\mu_H(0K, {p_0}^{H_2}) = \frac{1}{2}E_{(H_2)} \equiv 0$, we can get $\Delta\mu_H(T, {p_0}^{H_2})$. Similar to $\Delta\mu_H(T, {p_0}^{H_2})$, we can calculate the values of $\Delta\mu_{CH_4}(T, p)$ and $\Delta\mu_{H_2O}(T, p)$ as well.

$$\mu_H(T, {p_0}^{H_2}) = \frac{1}{2}[H(T, {p_0}^{H_2}) - H(0K, {p_0}^{H_2})] - \frac{1}{2}T[S(T, {p_0}^{H_2}) - S(0K, {p_0}^{H_2})] \quad (18)$$

Fig. 6(a) shows that in the absence of the electric field, ΔG for CH_xOH and CH_xO at 1000 K as a function of the hydrogen chemical potential. In order to prevent coking, experimenters keep the partial pressure ratio of H_2O/CH_4 to ~3 [68]. A lower value of ΔG indicates that the conformation is more stable on the Ni(111) surface. When the field is absent, the more hydrogenated species (CH_xOH) are stabilized as the hydrogen pressure is increased. When the hydrogen partial pressure is low, CO, CHO and COH are the most stable species on Ni(111). For high hydrogen partial pressure values, CH_3OH and CH_3O are more likely to stay on the surface. But under such high temperature conditions, it would be hard to obtain methanol as a product from the reactor since after its desorption, gas phase methanol decomposes easily into carbons and hydrogen gas [69]. It is also worth mentioning that even if we change the partial pressures or the H_2O/CH_4 ratio, the relative stabilities of the MSR-involved species won't change at a given temperature.

Fig. 7(a) and (c) separately present the relative equilibrium stabilities of CH_x and OH_y intermediates as the function of the hydrogen partial pressure with no electric fields. The results clearly show that at low partial pressures of hydrogen, we can obtain surface C atoms and CH molecules from the dissociation of pure methane, while a CH_3 molecule is more likely to occur on the surface as we increase the partial pressure of hydrogen above 5×10^6 Pa. For the dissociation of water, surface oxygen species are stable for low partial hydrogen pressure values, while hydroxyl species are more stable at high hydrogen partial pressures. By combining this information with the stability of CH_xOH_y species, we can conclude that at low partial pressures of hydrogen, we can obtain surface CO, CHO, COH, C, CH and O since they are stable under such applied conditions. Furthermore, under such conditions, a CO product can be formed from the surface oxygen oxidation of either an adsorbed C or a surface CH group. On the other hand, when the hydrogen partial pressure is higher than 5×10^6 Pa, the most stable species on the surface change to CH_3OH, CH_3O, CH_3, and OH. This suggests that under high hydrogen partial pressure conditions, the surface methanol species can be obtained from the oxidation of CH_3 with adsorbed hydroxyl groups.

For different hydrogen chemical potential values, an electric field will play different roles in the relative equilibrium stability of MSR-involved intermediates. When the hydrogen chemical potential value is low, a CO molecule on Ni(111) has the lowest value of ΔG. At these conditions, COH and CHO intermediates are also very stable on the surface as compared to the stabilities of other CH_xO and CH_xOH molecules. Moreover, due to the large differences of the ΔG values for each intermediate value of $\Delta\mu_H$, the electric field effects are not large enough to alter the order of stability for these intermediates. Similarly, in the absence of field, CH_3OH and CH_3O are more likely to be observed on Ni(111) when the hydrogen partial pressure is high. An electric field on the order of −1.0 V/Å to 1.0 V/Å also does not significantly affect the stability order for CH_xO and CH_xOH under these conditions. Similarly, when the hydrogen chemical potential value is very low or very high, an electric field did not alter the stability orders of CH_x and OH_y species as well.

On the other hand, at moderate hydrogen partial pressure values of ~10^6 Pa (Figs. 6(b), 7(b) and (d)), the presence of a simulated field can modify the relative stability of the adsorbates: (i) For the CH_xOH_y species, CO is the most favorable species on Ni(111) at negative field values, while methanol becomes much more stable over the surface as we increase the field value from negative to positive values; (ii) For the CH_x species, CH is the most stable species over a Ni surface, while CH_3 is the second most stable species and becomes much more stable as we apply a large positive electric field; (iii) For the OH_y species at a high positive electric field value at moderate hydrogen partial pressures, we can get hydroxyl groups on the Ni surface. As a result, the presence of a high positive electric field can aid in the formation of methanol on Ni(111) via the reaction of CH_3 species with hydroxyl groups under certain conditions.

3.4.2. Combining phase diagram with thermodynamic scheme

By combining our phase diagram (Figs. 6 and 7) and thermodynamic scheme (Figs. 8 and 9), we can better understand the underlying processes occurring during the MSR reaction. From Section 3.4.1, we know that CO has the lowest ΔG at low hydrogen chemical potential values in the absence of a field. The CO products can be obtained from the surface oxygen oxidation of either an adsorbed C or a surface CH group, since these species are thermodynamically stable on a Ni(111) surface under such conditions. Based on Fig. 8, the lowest energy pathway is shown in Eq. (19), which also includes CH, O, and CHO intermediates.

$$CH_4 + H_2O \rightarrow CH + O + 5H \rightarrow CHO + 5H \rightarrow CO + 6H \rightarrow CO + 3H_2 \quad (19)$$

We remark that the overall energy profile plotted in Figs. 8 and 9 for the MSR reaction are from DFT calculations at 0 K. However, after accounting the entropy effects (using an MSR operating temperature of 1073 K), the Gibbs free energy changes (ΔG) of a CO molecule from the Ni(111) surface to a gas phase CO molecule in the presence of a positive field, in the absence of a field and in the presence of a negative field are only −0.35 eV, −0.12 eV and 0.02 eV. We remark that the exothermic values are due to high temperatures involved since at room temperature these values would be 1.14 eV, 1.37 eV and 1.56 eV, respectively. Consequently, the overall MSR reaction energy profile, involving the production of CO and H_2 in the gas phase, reduces from ~3 eV (at 0 K) to ~2 eV (at 1073 K). On the other hand, for the surface reactions, such as $CH_x^* \rightarrow CH_{x-1}^* + H^*$, $CH_x^* + O^* \rightarrow CH_xO^*$, the entropy effects on the reaction energies at 1073 K are all less than 0.2 eV as compared to the ones at 0 K, which are significantly smaller than the phase change steps (i.e. the CO

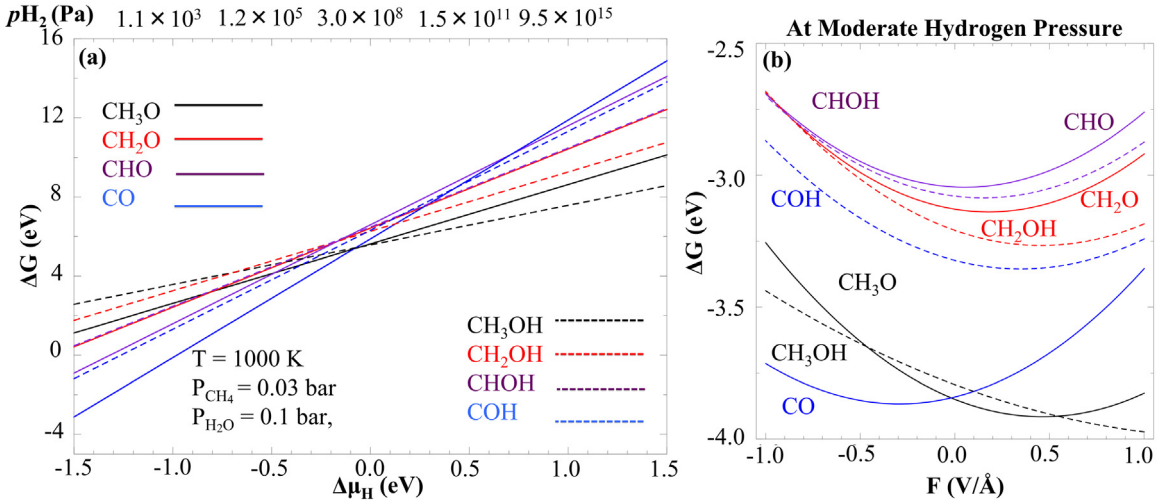

Fig. 6. Phase diagram from first principles representing the relative equilibrium stabilities of the CH_xO and CH_xOH species as a function of the hydrogen chemical potential and an electric field. Part (a) presents the value of ΔG as a function of hydrogen partial pressure with no fields. Part (b) shows that the Gibbs free energy of adsorption ΔG as a function of an electric field of −1 V/Å to 1 V/Å at hydrogen partial pressures of ~10^6 Pa. It is also worthy to mention that all the intermediates we identified here are at a low coverage of 1/9 ML.

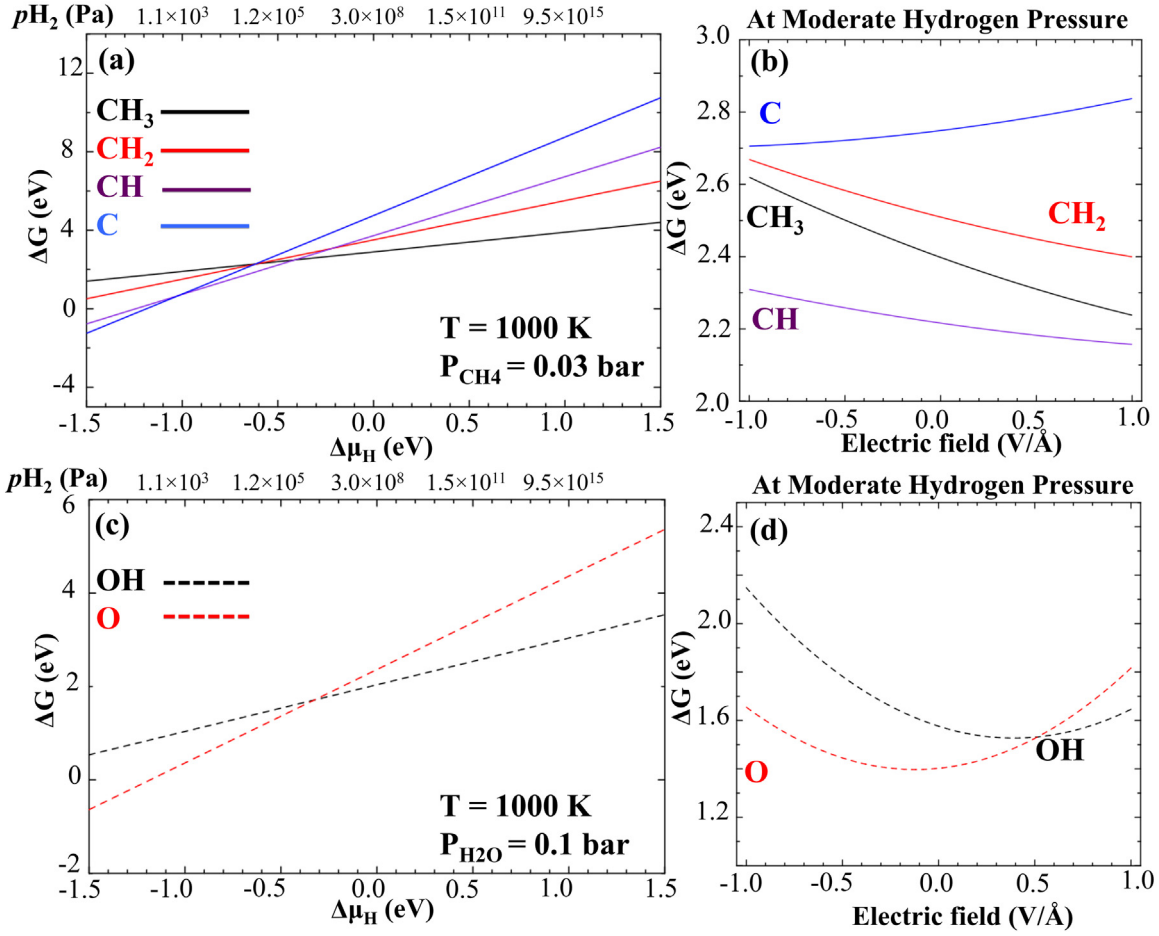

Fig. 7. The relative equilibrium stabilities of the CH_x and OH_x species as a function of the hydrogen chemical potential and an electric field. Part (a) presents the value of ΔG as a function of hydrogen partial pressure in the absence of a field. Part (b) shows ΔG, the Gibbs free energy of adsorption, as a function of an electric field of −1 V/Å to 1 V/Å at the same moderate hydrogen partial pressures (~10^6 Pa) that we presented in Fig. 7. It is also worthy to mention that all the intermediates we identified here are at a low coverage of 1/9 ML.

desorption) and will not largely influence the overall energy profiles. More details related to the Gibbs free energy calculations are given in Section 5 in the ESI.

Fig. 9(a) shows the simulated field effects on this lowest energy pathway. A positive field significantly strengthens the adsorption of reactants, decreases the desorption energy of the CO and H_2 prod-

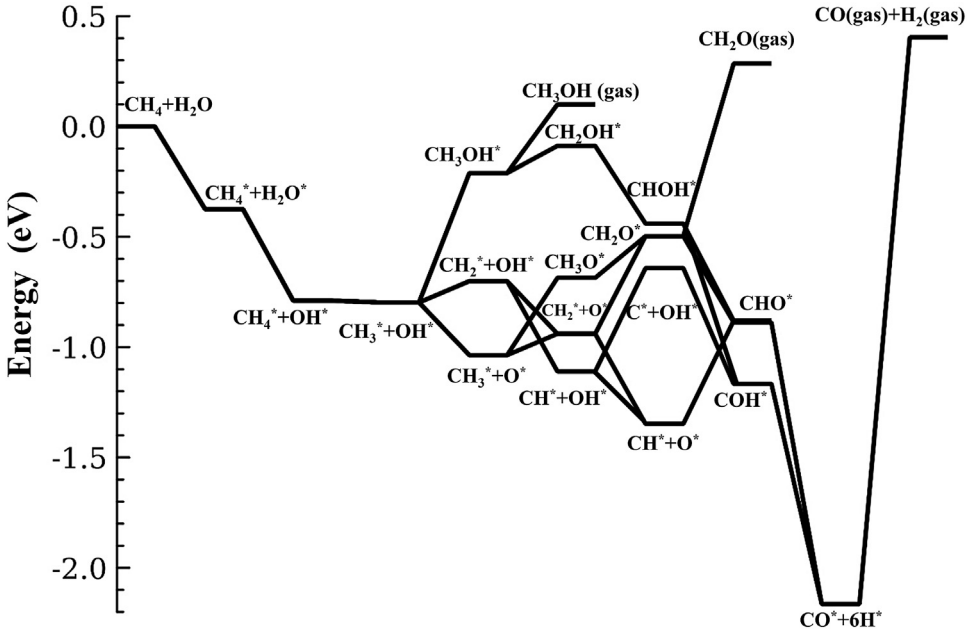

Fig. 8. Thermodynamic scheme of all possible mechanisms (see Fig. 1) in MSR reaction over a Ni(111) catalysts in the absence of a field. Here we use '*' to denote when the species are adsorbed on a Ni(111) surface.

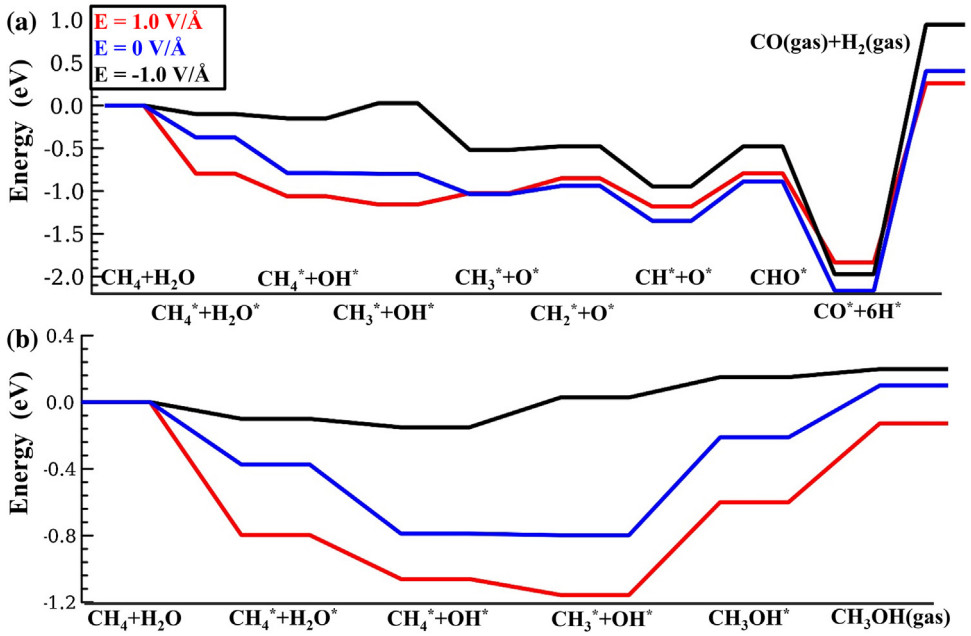

Fig. 9. The lowest energy pathway in the presence and absence of an electric field (a) and the reaction pathway for forming methanol via hydroxyl oxidation of CH_3 species (b).

ucts, and lowers the overall energy profile. Therefore, we conclude that a positive electric field improves the MSR processes. On the other hand, at moderate hydrogen partial pressure values ($\sim 10^6$ Pa) at field values ranging from 0.0 V/Å to 0.5 V/Å, we can obtain the surface CH_3O intermediate. Among the reaction mechanisms that involve the CH_3O intermediates, only the $CH_4 \rightarrow CH_3 + H$ and the $CH_3 + O \rightarrow CH_3O$ reactions are endothermic. A positive electric field also further decreases the reaction energies of these two reactions and causes these two reactions to become slightly exothermic. Thus, from the perspective of only the reaction energy, the CH_3O-involved reaction mechanisms are likely to occur in the presence of a positive field ranging from 0.0 V/Å to 0.5 V/Å and at moderate hydrogen partial pressure values. Additionally, after increasing the field from 0.5 V/Å to 1 V/Å, we can obtain methanol on Ni(111). From Fig. 9(b), it is also clearly shown that the presence of a positive field can lower the overall energy profile of forming methanol. This information can help us select a reduced number of elementary reactions from such a potentially complex overall MSR reaction mechanism when calculating reaction energy barriers, as shown in Fig. 1.

4. Conclusion

We thoroughly investigated the effect of an electric field on the adsorption the MSR-involved species as well as its influence on the reaction energies of all possible MSR elementary reactions. In our adsorption study in the presence of a simulated field we found that the effect of an electric field on MSR-involved chemisorbed species are similar. Such a conclusion was obtained through our projected density of states, differential charge density and Bader charge analysis. The field-dependent adsorption strength of MSR intermediates based on the effective dipole moment analysis was found to be as follows: $CH_xO > CH_xOH > H_xO > CH_x$. On the other hand, the formation of CH_xO and CH_xOH was found to be more rates dominating than their corresponding dehydrogenation reactions. With a positive field, surface O atom oxidation of CH_x species is more likely to occur, while with a negative field, surface hydroxyl group oxidation of CH_x is more likely to occur.

The phase diagram that was constructed from first principles provides the relative equilirium stabilities of the possible MSR intermediates as a function of both the hydrogen partial pressure and a tunable electric field strength under realistic experimental conditions. This provides us the most likely occurring MSR mechanisms at moderate hydrogen partial pressures, where CO can be obtained with a negative field, while the CH_3OH can be found over the surface for positive field values. For the most favorable reaction methanisms with different hydrogen pressures, the overall energy profiles are further lowered in the presence of a positive electric field. In summary, our computational results enhance our understanding of the catalytic MSR reaction mechanisms in the presence of tunable electric fields. The information provided here also points us toward the selection of the elementary reactions for further kinetic studies of the methane steam reforming reaction mechanism. By combing this study with our previous work, we conclude that a positive electric field can significantly reduce the formation of coke, lower the lowest energy path, stabilize the adsorption of reactants, and assist the desorption of products on a Ni catalyst. For the future work, it is necessary to establish a microkinetic model for such a catalytic MSR reaction with tunable electric fields in order to capture the electric field effects for the conversion of methane during the MSR process, the temperature requirements of the said reaction, the coke formation and the identification of intermediates as a function of time. The established microkinetic model would then guide the design of new Ni-based electrocatalytic methane steam reforming catalysts with lower operating temperatures and higher coke resistance.

Acknowledgments

We gratefully acknowledge our support by institutional funds provided to JSM from the Voiland School of Chemical Engineering and Bioengineering. We also thanks to USDA/NIFA that partial work was under support through the Hatch Project #WNP00807 titled: “Fundamental and Applied Chemical and Biological Catalysts to Minimize Climate Change, Create a Sustainable Energy Future, and Provide a Safer Food Supply”. Our thanks also go to the donors of The American Chemical Society Petroleum Research Fund for partial support. Furthermore, parts of our computational resources were provided by the Center for Nanoscale Materials at Argonne National Laboratory. Use of the Center for Nanoscale Materials was supported by the U.S. Department of Energy, Office of Science, Office of Basic Energy Sciences. We also acknowledge Mr. Gregory B. Collinge for his helpful comments.

Appendix A. Supplementary data

Supplementary data associated with this article can be found, in the online version, at http://dx.doi.org/10.1016/j.apcatb.2016.04.026.

References

[1] A.B. Stambouli, E. Traversa, Renew. Sustai. Energy Rev. 6 (2002) 433–455.
[2] J. Sun, X.-P. Qiu, F. Wu, W.-T. Zhu, Int. J. Hydrogen Energy 30 (2005) 437–445.
[3] M.L. Andrade, L. Almeida, M. do Carmo Rangel, F. Pompeo, N. Nichio, Chem. Eng. Technol. 37 (2014) 343–348.
[4] B.V. Merinov, J.E. Mueller, A.C.T. van Duin, Q. An, W.A. Goddard, J. Phys. Chem. Lett. 5 (2014) 4039–4043.
[5] D. Mogensen, J.D. Grunwaldt, P.V. Hendriksen, K. Dam-Johansen, J.U. Nielsen, J. Power Sources 196 (2011) 25–38.
[6] M. Andersson, H. Paradis, J. Yuan, B. Sundén, Int. J. Energy Res. 35 (2011) 1340–1350.
[7] D. Pakhare, J. Spivey, Chem. Soc. Rev. 43 (2014) 7813–7837.
[8] S.D. Angeli, G. Monteleone, A. Giaconia, A.A. Lemonidou, Int. J. Hydrogen Energy 39 (2014) 1979–1997.
[9] K. Supat, S. Chavadej, L.L. Lobban, R.G. Mallinson, Ind. Eng. Chem. Res. 42 (2003) 1654–1661.
[10] J. Sehested, J.A.P. Gelten, I.N. Remediakis, H. Bengaard, J.K. Nørskov, J. Catal. 223 (2004) 432–443.
[11] J. Sehested, Catal. Today 111 (2006) 103–110.
[12] K. Ahmed, K. Foger, Catal. Today 63 (2000) 479–487.
[13] J. Liu, B.D. Madsen, Z. Ji, S.A. Barnett, Electrochem. Solid-State Lett. 5 (2002) A122–A124.
[14] M.N. Barroso, A.E. Galetti, M.C. Abello, Appl. Catal. A 394 (2011) 124–131.
[15] S. Adhikari, S. Fernando, S.R. Gwaltney, S.D. Filip To, R. Mark Bricka, P.H. Steele, A. Haryanto, Int. J. Hydrogen Energy 32 (2007) 2875–2880.
[16] A.M. Gadalla, B. Bower, Chem. Eng. Sci. 43 (1988) 3049–3062.
[17] S. Adhikari, S. Fernando, A. Haryanto, Energy Fuels 21 (2007) 2306–2310.
[18] K. Hou, R. Hughes, Chem. Eng. J. 82 (2001) 311–328.
[19] J. Comas, F. Mariño, M. Laborde, N. Amadeo, Chem. Eng. J. 98 (2004) 61–68.
[20] G. Jones, J.G. Jakobsen, S.S. Shim, J. Kleis, M.P. Andersson, J. Rossmeisl, F. Abild-Pedersen, T. Bligaard, S. Helveg, B. Hinnemann, J.R. Rostrup-Nielsen, I. Chorkendorff, J. Sehested, J.K. Nørskov, J. Catal. 259 (2008) 147–160.
[21] H.S. Bengaard, J.K. Nørskov, J. Sehested, B.S. Clausen, L.P. Nielsen, A.M. Molenbroek, J.R. Rostrup-Nielsen, J. Catal. 209 (2002) 365–384.
[22] R.C. Weast, CRC Handbook of Chemistry and Physics, CRC Press Boca Raton, FL, 1983.
[23] D.W. Blaylock, T. Ogura, W.H. Green, G.J.O. Beran, J. Phys. Chem. C 113 (2009) 4898–4908.
[24] J.R. Rostrup-Nielsen, Phys. Chem. Chem. Phys. 3 (2001) 283–288.
[25] S.-G. Wang, X.-Y. Liao, J. Hu, D.-B. Cao, Y.-W. Li, J. Wang, H. Jiao, Surf. Sci. 601 (2007) 1271–1284.
[26] C.F. Gorin, E.S. Beh, M.W. Kanan, J. Am. Chem. Soc. 134 (2012) 186–189.
[27] Y. Sekine, M. Haraguchi, M. Tomioka, M. Matsukata, E. Kikuchi, J. Phys. Chem. A 114 (2009) 3824–3833.
[28] Y. Sekine, M. Haraguchi, M. Matsukata, E. Kikuchi, Catal. Today 171 (2011) 116–125.
[29] F. Che, R. Zhang, A.J. Hensley, S. Ha, J.-S. McEwen, Phys. Chem. Chem. Phys. 16 (2014) 2399–2410.
[30] F. Che, A.J. Hensley, S. Ha, J.-S. McEwen, Catal. Sci. Technol. 4 (2014) 4020–4035.
[31] F. Che, J.T. Gray, S. Ha, J.-S. McEwen, J. Catal. 332 (2015) 187–200.
[32] J. Neugebauer, M. Scheffler, Phys. Rev. B 46 (1992) 16067–16080.
[33] J.-S. Filhol, M. Neurock, Angew. Chem. Int. Ed. 45 (2006) 402–406.
[34] C.D. Taylor, S.A. Wasileski, J.-S. Filhol, M. Neurock, Phys. Rev. B 73 (2006) 165402.
[35] H.J. Kreuzer, R.L.C. Wang, Philos. Mag. B 69 (1994) 945–955.
[36] G. Pacchioni, J.R. Lomas, F. Illas, J. Mol. Catal. A: Chem. 119 (1997) 263–273.
[37] E.M. Stuve, Chem. Phys. Lett. 519-520 (2012) 1–17.
[38] K.Y. Yeh, M.J. Janik, in: A. Asthagiri, M.J. Janik (Eds.), Computational Catalysis. The Royal Society of Chemistry, 2014, pp. 116–156.
[39] K.-Y. Yeh, S.A. Wasileski, M.J. Janik, Phys. Chem. Chem. Phys. 11 (2009) 10108–10117.
[40] A.E. Bolzán, A.C. Chialvo, A.J. Arvia, J. Electroanal. Chem. Interfacial Electrochem. 179 (1984) 71–82.
[41] K. Walter, O.V. Buyevskaya, D. Wolf, M. Baerns, Catal. Lett. 29 (1994) 261–270.
[42] D. Qin, J. Lapszewicz, X. Jiang, J. Catal. 159 (1996) 140–149.
[43] E. Shustorovich, ChemInform. 22 (1991) 310.
[44] J. Wellendorff, T.L. Silbaugh, D. Garcia-Pintos, J.K. Nørskov, T. Bligaard, F. Studt, C.T. Campbell, Surf. Sci. 640 (2015) 36–44.
[45] J. White, D. Bird, Phys. Rev. B 50 (1994) 4954–4957.
[46] J.P. Perdew, K. Burke, M. Ernzerhof, Phys. Rev. Lett. 77 (1996) 3865–3869.
[47] J.P. Perdew, Y. Wang, Phys. Rev. B 45 (1992) 13244–13249.
[48] M.C. Payne, T.A. Arias, J.D. Joannopoulos, Rev. Mod. Phys. 64 (1992) 1045–1097.
[49] P.J. Feibelman, Phys. Rev. B 64 (2001) 125403.

[50] S. Grundner, M.A.C. Markovits, G. Li, M. Tromp, E.A. Pidko, E.J.M. Hensen, A. Jentys, M. Sanchez-Sanchez, J.A. Lercher, Nat. Commun. 6 (2015).
[51] E. Masumian, S.M. Hashemianzadeh, A. Nowroozi, Phys. Lett. A 378 (2014) 2549–2552.
[52] J.S. McEwen, P. Gaspard, T. Visart de Bocarmé, N. Kruse, J. Phys. Chem. C 113 (2009) 17045–17058.
[53] J.S. Filhol, M.L. Doublet, J. Phys. Chem. C 118 (2014) 19023–19031.
[54] J.-S. Filhol, M.-L. Doublet, Catal. Today 202 (2013) 87–97.
[55] J.S. Filhol, M.L. Bocquet, Chem. Phys. Lett. 438 (2007) 203–207.
[56] R.F.W. Bader, In Atoms in Molecules: A Quantum Theory, Oxford University Press, Oxford, 1990.
[57] J.N. Bronsted, Chem. Rev. 5 (1928) 231–338.
[58] R.P. Bell, Proc.—R. Soc. London Sect. A: Math. Phys. Sci 154 (1936) 414–429.
[59] Evans, M. Polanyi, Trans. Faraday Soc. 32 (1936) 1333–1360.
[60] A.L.J. Beckwith, Chem. Soc. Rev. 22 (1993) 143–151.
[61] J.E. Sutton, D.G. Vlachos, ACS Catal. 2 (2012) 1624–1634.
[62] R.A.v. Santen, M. Neurock, S.G. Shetty, Chem. Rev. 110 (2010) 2005–2048.
[63] J.S. McEwen, T. Anggara, W.F. Schneider, V.F. Kispersky, J.T. Miller, W.N. Delgass, F.H. Ribeiro, Catal. Today 184 (2012) 129–144.
[64] K. Reuter, C. Stampf, M. Scheffler, in: S. Yip (Ed.), Hand-book of Materials Modeling, Springer Netherland, 2005, pp.149–194.
[65] R.B. Getman, Y. Xu, W.F. Schneider, J. Phys. Chem. C 112 (2008) 9559–9572.
[66] K. Reuter, M. Scheffler, Phys. Rev. B 65 (2001) 035406.
[67] JANAF thermochemical tables, D.R. Stull and H. Prophet, project directors, U.S. Dept. of Commerce, National Bureau of Standards, Washington, D.C, 1971.
[68] A.L. Dicks, K.D. Pointon, A. Siddle, J. Power Sources 86 (2000) 523–530.
[69] Y. Matsumura, N. Tode, Phys. Chem. Chem. Phys. 3 (2001) 1284–1288.